Research Paper

The complexity of sediment recycling as revealed by common Pb isotopes in K-feldspar

Check for updates

Simon P. Johnson [a,*], Christopher L. Kirkland [b], Noreen J. Evans [c], Brad J. McDonald [c], Huntly N. Cutten [a]

[a] Geological Survey of Western Australia, Mineral House, 100 Plain Street, East Perth, Western Australia, 6004, Australia
[b] Centre for Exploration Targeting — Curtin Node, The Institute for Geoscience Research, Department of Applied Geology, Western Australian School of Mines, Curtin University, Perth, Western Australia, 6102, Australia
[c] John de Laeter Centre, The Institute for Geoscience Research, Department of Applied Geology and Applied Physics, Curtin University, Perth, Western Australia, 6102, Australia

ARTICLE INFO

ABSTRACT

Detrital zircon U—Pb geochronology has become the gold standard in evaluating source to sink relationships in sedimentary basins. However, the physical and chemical robustness of zircon, which make it such a useful mineral for provenance studies, is also a hindrance as zircon can be recycled through numerous sedimentary basins, thus obscuring the first cycle source to sink relationship. An elegant approach to addressing this potential issue is to compare the Pb isotope composition of detrital K-feldspar, a mineral which is unlikely to survive more than one erosion-transport-deposition cycle, with that of magmatic K-feldspar from potential basement source terranes. Here we present new in situ Pb isotope data on detrital K-feldspar from two Proterozoic arkosic sandstones from Western Australia, and magmatic K-feldspar grains from potential igneous source rocks, as inferred by the age and Hf isotope composition of detrital zircon grains. The data indicate that the detrital zircon and K-feldspar grains could not have been liberated from the same source rocks, and that the zircon has most likely been recycled through older sedimentary basins. These results provide a more complete understanding of apparently simple source to sink relationships in this part of Proterozoic Western Australia.

1. Introduction

Comparing the age and chemical or isotopic signature of minerals in sedimentary rocks to those in potential basement hinterlands is a fundamental tool used to fingerprint source to sink relationships. Such source to sink relationships provide many key constraints used to test palaeogeographic models, refine stratigraphy, and potentially understand depositional timeframes. Detrital zircon geochronology has evolved as the choice for provenance studies because zircon grains are ubiquitous in sandstones, highly resistant to both chemical and physical weathering, amenable to U—Pb dating and carry other isotopic and chemical signatures (e.g. Lu—Hf, REE) that may uniquely link a zircon grain to its basement source. However, although the refractory nature of zircon provides the benefit of recording much of the high-temperature history of a geological terrane, its resistance to erosion provides a challenge to provenance reconstruction as it can be recycled a multitude of times. The (U—Th)/He and U—Pb 'double' dating of detrital zircons from a number of sedimentary basins (e.g. Rahl et al., 2003; Campbell et al., 2005) has showed that many zircon grains were exposed to the surface environment long before their host sedimentary rocks have been deposited. In many cases, a major source of sediment detritus is uplift, erosion and recycling of pre-existing (meta)-sedimentary basins. The longevity of the sedimentary cycle means that apparent direct source to sink pathways may, in reality, be much more cryptic (Dickinson et al., 2009; Dickinson and Gehrels, 2009; Hadlari et al., 2015; Anderson et al., 2016), particularly in Precambrian (meta)-sedimentary basins which are commonly deformed or metamorphosed and where other indicators of source provenance, such as paleoflow structures are obscured or obliterated.

* Corresponding author.
E-mail address: simonpaul.johnson@dmirs.wa.gov.au (S.P. Johnson).
Peer-review under responsibility of China University of Geosciences (Beijing).

One elegant approach to address the primary source to sink relationship is to compare the common Pb isotopic signature of detrital K-feldspar, a mineral unlikely to survive more than one erosion-transport-deposition cycle, with the signature of potential source basement terranes (e.g. Tyrrell et al., 2006, 2007, 2009, 2012; Flowerdew et al., 2012; Zhang et al., 2014, 2016, 2017; Gagnevin et al., 2017; Lancaster et al., 2017; Reat et al., 2017). K-feldspar is a common mineral in many clastic rocks and is a major constituent of arkosic sandstones. It usually has appreciable concentrations of Pb (10–40 ppm) and little to no U or Th, so there is minimal post-crystallization contamination of radiogenic Pb, which can obscure primary ratios. Furthermore, the Pb isotopic signature in detrital feldspar has been shown to be retained despite recrystallization associated with diagenesis (Tyrrell et al., 2006). Lead isotope variations ($^{206}Pb/^{204}Pb$, $^{207}Pb/^{204}Pb$ and $^{208}Pb/^{204}Pb$) in igneous and metamorphic crustal rocks define broad spatial patterns that make the Pb signature of detrital K-feldspar grains a useful provenance tool (e.g. Tyrrell et al., 2012; Flowerdew et al., 2013; Lancaster et al., 2017). Regional patterns in Pb isotopic composition can be identified by characterizing a relatively small number of feldspar grains from potential granitic basement sources (Zartmann and Wasserburg, 1969; DeWolf and Mezger, 1994), or by analysing Pb variations in galena (Fletcher and Farquhar, 1982; Dixon et al., 1990).

The Paleo- to Mesoproterozoic Edmund Group in the Capricorn Orogen of Western Australia is dominated by sandstone units containing detrital zircons that are similar in age and isotopic composition to the underlying basement magmatic rocks of the Gascoyne Province (Martin et al., 2008; Cutten et al., 2016).

However, abundant, well-developed paleoflow indicators throughout the basin suggest a primary source outside the province (Martin et al., 2008), implying that the zircon detritus has been recycled, presumably through older basins (Cutten et al., 2016). Here we report the common Pb isotopic signature of detrital K-feldspar from two arkosic sandstones in the Edmund Group, and compare the results to the composition of magmatic K-feldspar from various basement granitic rocks in order to address this dichotomy and further elucidate source to sink relationships in this basin.

2. Geological setting

The Capricorn Orogen is a ~1000 km long, ~500 km wide zone located between the Archean Yilgarn and Pilbara Cratons of Western Australia. The orogen comprises the deformed margins of the two Archean cratons, Proterozoic granitic and metasedimentary rocks of the Gascoyne Province as well as numerous, variably deformed Proterozoic sedimentary basins including the Paleo- to Mesoproterozoic Edmund Basin (Fig. 1; Martin and Thorne, 2004; Martin et al., 2008; Cutten et al., 2016). The orogen formed during the punctuated assembly of the Yilgarn and Pilbara Cratons to form the larger West Australian Craton (e.g. Johnson et al., 2013), and has subsequently been the site of repeated intraplate reworking spanning over one billion years (Sheppard et al., 2005, 2007; Korhonen et al., 2017). The province is dominated by medium- to coarse-grained felsic magmatic rocks of the 1820–1775 Ma Moorarie Supersuite and the 1680–1620 Ma Durlacher Supersuite. Following the emplacement of the Durlacher
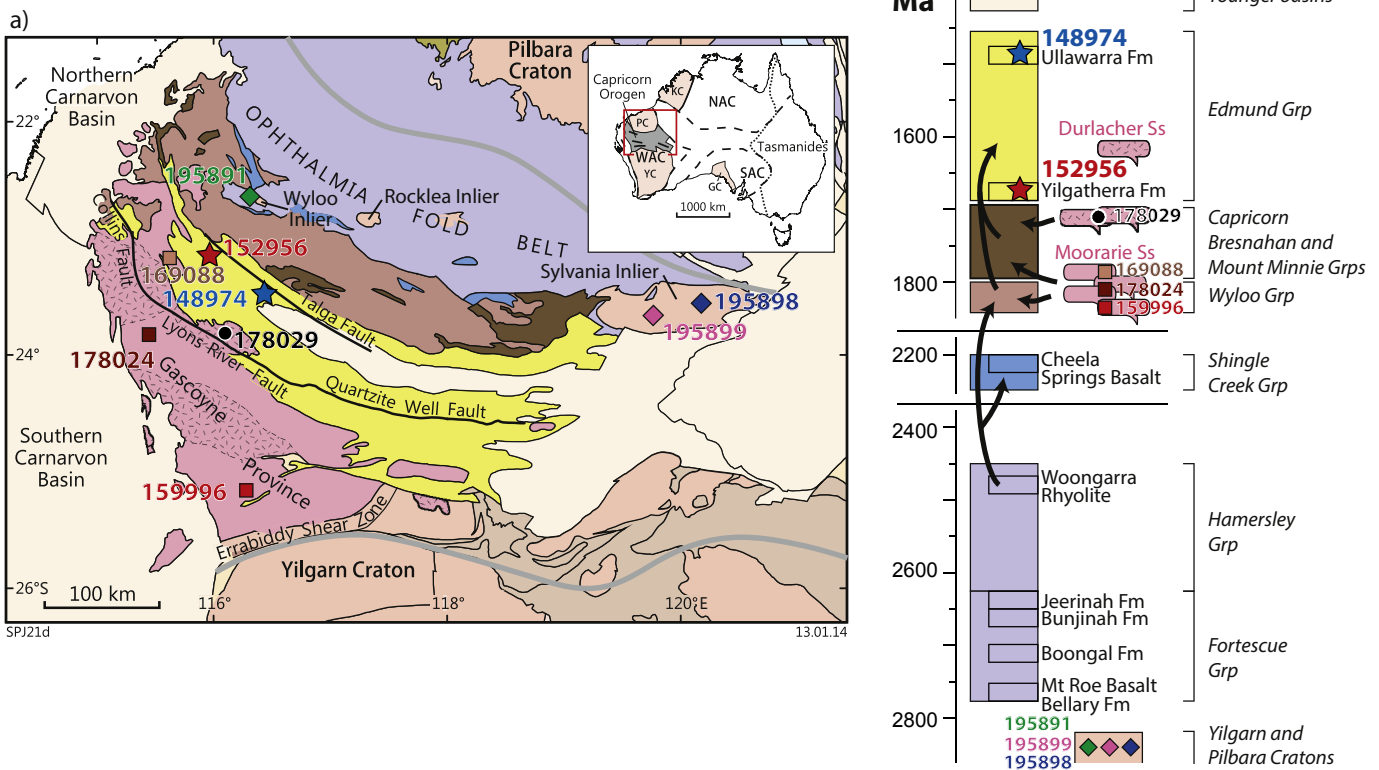
Figure 1. (a) Simplified geological map of the Capricorn Orogen of Western Australia, showing the location of samples studied. The geological legend is provided as a stratigraphic column in (b) which shows possible pathways for recycling of detrital zircons. Inset in (a) is a simplified tectonic map of Australia. Abbreviations: GC—Gawler Craton; KC—Kimberley Craton; NAC—North Australian Craton; PC—Pilbara Craton; SAC—South Australian Craton; WAC—West Australian Craton; YC—Yilgarn Craton.

Supersuite, the province displays a broad secular change to more rigid behaviour (Johnson et al., 2017), allowing the emplacement of abundant mafic dykes and sills into the shallow crust (Wingate, 2002; Morris and Pirajno, 2005), and the formation of thick intracontinental sedimentary basins, including the deposition of the 1673–1455 Ma Edmund Group into the Edmund Basin (Fig. 1; Martin and Thorne, 2004; Martin et al., 2008; Cutten et al., 2016).

The Edmund Group is a mixed siliciclastic and carbonate sedimentary unit up to 9.5 km thick, comprising predominantly sandstone and siltstone, with subordinate conglomerate, dolostone, stromatolitic dolostone, carbonaceous siltstone and chert (Martin and Thorne, 2004). The sedimentary rocks were deposited in a variety of fluvial to marine shelf or basinal environments (Martin and Thorne, 2004; Martin et al., 2008; Cutten et al., 2016), the distribution of which was strongly controlled by fluctuations in relative sea-level and syn-sedimentary movement on major, pre-existing basement faults (Cutten et al., 2016). The group has been divided into four, informal depositional packages that includes 11 formations, from base to top: the Yilgatherra, Irregularly, Gooragoora, Blue Billy, Cheyne Springs, Kiangi Creek, Muntharra, Discovery, Devil Creek, Ullawarra and Coodardoo formations (Fig. 2; Martin and Thorne, 2004). Each package is defined by a basal unconformity or a major marine flooding surface, both of which are the result of differential fault movements or fluctuations in sea level (Martin and Thorne, 2004). A more detailed description of

individual lithologies and the facies distribution for each formation is provided by Martin and Thorne (2004), Martin et al. (2008) and Cutten et al. (2016). At various times, parts of the group were intruded by voluminous mafic sills of the 1517–1505 Ma Waldburg Dolerite (Blay et al., 2015), the 1465–1452 Ma Narimbunna Dolerite (Wingate, 2002), and the 1084–1067 Ma Kulkatharra Dolerite (Wingate, 2002), which may have locally inflated the stratigraphic thickness by as much as 60% (Morris and Pirajno, 2005). Following deposition, all rocks within the basin were subject to locally intense faulting and folding during the 1321–1171 Ma Mutherbukin Tectonic Event (Cutten et al., 2016; Korhonen et al., 2017) and the 1029–954 Ma Edmundian Orogeny (Sheppard et al., 2007; Cutten et al., 2016). Despite this locally intense deformation, the preservation of well-defined paleoflow indicators such as trough cross bedding and sole marks indicate that much of the sediment throughout the group was derived from a northerly source region rather than the underlying Gascoyne Province that is exposed to the south (Martin et al., 2008; Cutten et al., 2016, Fig. 2).

3. Materials and methods

Light fractions from previous heavy mineral separation were utilized to produce a 25 mm epoxy resin mount for each sample that was polished to expose interiors of grains at approximately half grain thickness. A Tescan TIMA, automated quantitative
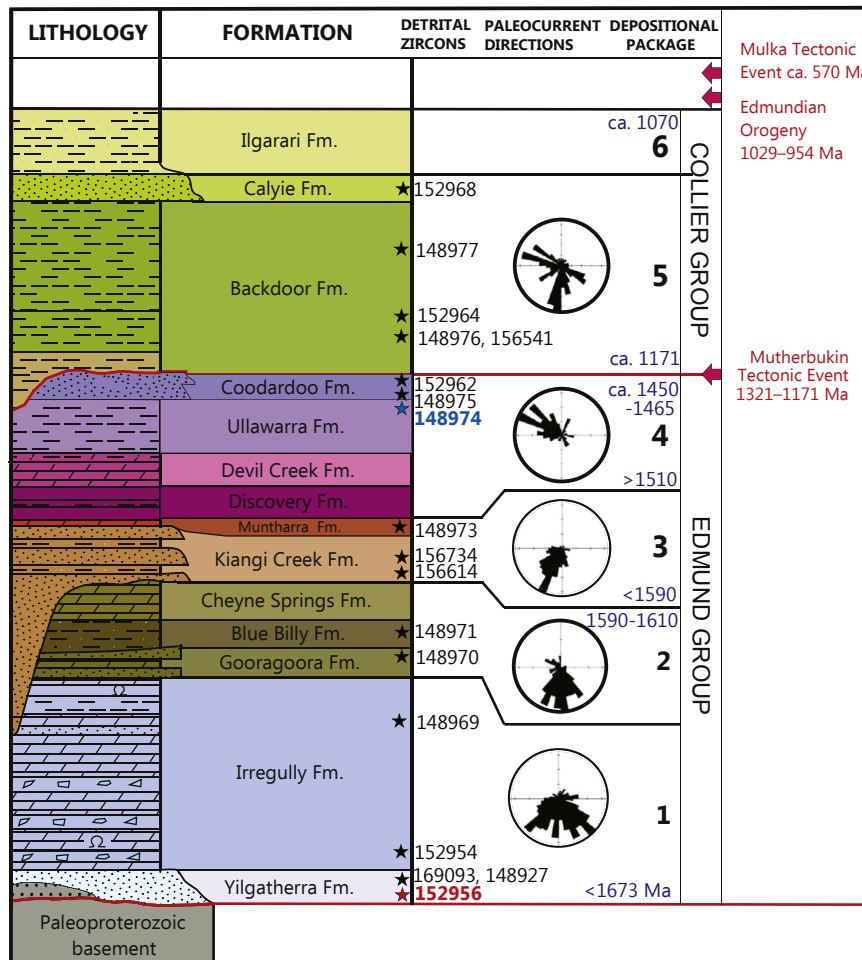
Figure 2. Stratigraphy of the Edmund and Collier Groups (after Cutten et al., 2016) showing subdivision into informal depositional packages and formations. The location of samples in this study (coloured) as well as those from Martin et al. (2008) are shown along with the timing of tectonic events and rose diagrams showing paleocurrent directions for each of the depositional packages. Geochronological constraints for the age of deposition are provided in Cutten et al. (2016) and Zi et al. (2015).

petrological analyser, based around a scanning electron microscope with an array of EDX detectors, was used to characterize the light mineral fraction from the granite and sandstone samples prior to isotopic analysis, and to produce both phase maps and backscatter electron images. This imaging process allows identification of areas that are altered, likely to have insufficient Pb (e.g. albite-rich lamellae in perthites; Housh and Bowring, 1991), or are rich in inclusions, particularly those with high U and Th contents that would have a deleterious effect on the measured common Pb ratios.

The Pb isotope composition of K-feldspar was determined using a laser ablation−multi-collector inductively coupled plasma mass spectrometry (LA-MC-ICPMS) during two sessions at the Geo-History Facility, John de Laeter Centre, Curtin University, Perth. The analyses were carried out on a Nu Plasma II (NPII) multi-collector mass spectrometer used in conjunction with a Resonetics S-155-LR 193 nm excimer laser ablation system. Operating conditions during the two session were identical. Standards and K-feldspar grains mounted and polished in epoxy rounds were spot ablated using a 50 μm beam diameter. The laser fluence (measured at sample surface) was 2 J/cm^2 and a pulse frequency of 10 Hz was utilized. Acquisition consisted of 40 s of baseline signal (no ablation) before target ablation and 20 s of baseline collection after target ablation. Two cleaning pulses were applied prior to the start of analysis. The sample cell was flushed with ultrahigh purity He (350 mL/min) and N$_2$ (1.0 mL/min) and high purity Ar was employed as the plasma carrier gas. Spot locations were chosen to avoid any heterogeneities (alteration, cracks, inclusions) identified on TIMA images. With these constraints, analysis was limited to a single spot per grain. Mass stations on the NPII were set as follows: ^{200}Hg, ^{202}Hg, ^{203}Ti, ^{204}Pb + ^{204}Hg on ion counters; ^{205}Tl, ^{206}Pb, ^{207}Pb, and ^{208}Pb on Faraday cups with a 0.8 s integration time for all. The 204 signal size for an unknown was typically 7 times the baseline signal (0.00003 V) on the ion counter. The monitoring of Hg allowed for three independent corrections for isobaric interference on mass 204, and Tl isotopes were monitored as they provide an option for an alternate method of mass fractionation quantification. In this work, however, downhole fractionation was corrected using matrix matched Shap feldspar (Tyrrell et al., 2006), analysed every 12 unknowns in a block with NIST 612 glass ($n = 50$ for all standards over the two sessions). Data was reduced using Iolite 3.5 using an in-house data reduction scheme that yields Pb isotopic ratios (Shap feldspar primary reference material) and an estimated Pb content (calculated using NIST 612 as the primary reference material). Shap feldspar, and NIST 612 treated as unknowns, yielded isotopic ratios within uncertainty of the recommended values during both analytical sessions (Woodhead and Hergt, 2001; Tyrrell et al., 2006). The standard data are provided in Supplementary Table 1. Corrected Pb isotope data for the detrital and magmatic grains are provided in Table 1.

4. Samples and results

Detrital K-feldspar from two samples of arkosic sandstone from the Edmund Group and magmatic K-feldspar from four samples of felsic magmatic rocks from the underlying Gascoyne Province and three from the northern Capricorn Orogen were analysed for their Pb isotope compositions. A total of 211 Pb isotopic analyses were collected from 211 K-feldspar crystals. Zones of alteration and inclusions identified by SEM-imaging were avoided during the laser ablation. Analytical results are shown in Fig. 3 and Table 1.

4.1. Detrital K-feldspar from the Edmund Group

Two samples of arkosic sandstone from the Edmund Group were selected for analyses as they contained abundant, unaltered detrital K-feldspar grains. Sample 152956 was collected from toward the base of the Edmund Group, from the Yilgatherra Formation of Depositional package 1 and sample 148974 from toward the top of the group, from the Ullawarra Formation (Curran Member) of Depositional package 4 (Fig. 2). Both samples contained abundant detrital zircon with prominent age modes suggesting derivation from the underlying Gascoyne Province magmatic rocks (Martin et al., 2008; Cutten et al., 2016).

4.1.1. 152956 − sandstone (Yilgatherra Formation)

This sample was collected approximately 2 m above the base of the Yilgatherra Formation and is a very coarse-grained, poorly sorted, trough-cross stratified, quartz-rich sandstone consisting predominantly of quartz (83%), K-feldspar (5%−7%), tourmaline (2%−3%), and muscovite (1%), with trace amounts of apatite and zircon (Martin et al., 2008). This sample was deposited in a high-energy fluvial system most likely from a large-scale braided river system (Martin et al., 2008). Trough cross stratification at this site suggests paleoflow from the northwest (Martin et al., 2008). U−Pb geochronology of detrital zircons yielded a range of dates between ca. 2762 Ma and 1733 Ma, with a major age mode yielding a weighted mean ^{207}Pb*/^{206}Pb* date of 1805 ± 9 Ma (Fig. 4a; Martin et al., 2008; Cutten et al., 2016). The zircons have a range of $\varepsilon_{Hf}(i)$ compositions between 1.4 and −9.5 (Fig. 5; Cutten et al., 2016). The combined U−Pb and Hf isotope data from these detrital zircons are consistent with their derivation from evolved crustal rocks of the Gascoyne Province (Fig. 4a and b).

TIMA classification of the light fraction indicates that the sample is dominated by quartz with minor orthoclase and muscovite. Orthoclase has a median grain size of 67 μm, although many grains are much smaller, and the grains are homogeneous. A total of 14 analyses were conducted on 14 orthoclase grains. ^{206}Pb/^{204}Pb ratios range from 16.5 to 20.5 with a median of 18.6. ^{207}Pb/^{204}Pb ratios range from 15.5 to 16.1 with a median of 15.8. ^{208}Pb/^{204}Pb ratios range from 36.4 to 42.3 with a median of 38.5 (Fig. 3).

4.1.2. 148974 − lithic sandstone (Curran Member, Ullawarra Formation)

This sample was taken from a unit of interbedded lithic turbidite sandstone and siltstone within the Curran Member of the Ullawarra Formation close to the top of the Edmund Group (Fig. 2; Martin et al., 2008). The sample is a fine-grained lithic turbidite sandstone that has no internal stratification or grading, is rich in poorly sorted silt to medium sand-sized detrital grains (35%−40%), and has a clay-rich matrix (Martin et al., 2008). The grains are mostly single-crystal quartz crystals 0.05−0.5 mm in diameter (35%), with lesser lithic fragments (10%), rare plagioclase and microcline (<1% each), and accessory muscovite, biotite, chlorite, leucoxene, rutile, anatase, and tourmaline. The Curran Member differs from the Ullawarra Formation only in the proportion of sandstone. This sample was most likely deposited in a deep-marine shelf environment, with the higher proportion of sandstone suggesting deposition during a period of significantly increased siliciclastic sediment supply (Martin et al., 2008). The mean paleoflow direction for the turbiditic sandstone units within the Curran Member is from the southeast (Fig. 2) and may reflect axial flow within the basin. U−Pb geochronology of detrital zircons yielded a range of dates between ca. 3064 Ma and 1618 Ma, with two prominent Proterozoic age modes yielding weighted mean ^{207}Pb*/^{206}Pb* dates of 1798 ± 5 Ma and 1680 ± 8 Ma (Martin et al., 2008), similar in age to the two main granitic supersuites in the underlying Gascoyne Province (Fig. 4a). For these two prominent Proterozoic age modes, the zircons yielded a range of $\varepsilon_{Hf}(i)$ compositions between 6.7 and −6.0 (Fig. 5; Cutten et al., 2016) consistent with this interpretation. However, the older zircons in the sample yielded

Table 1
Lead isotope data for feldspars from sediment and basement rocks of the Capricorn Orogen. Lead isotope data have been corrected for fractionation.

Sample	$^{206}Pb/^{204}Pb$	$\pm 2\sigma$	$^{207}Pb/^{204}Pb$	$\pm 2\sigma$	$^{208}Pb/^{204}Pb$	$\pm 2\sigma$	Pb (ppm)	$\pm 2\sigma$
1679—1455 Ma Edmund Group sedimentary rocks								
152956—sandstone (Yilgatherra Formation)								
6	16.49	0.13	15.65	0.16	36.35	0.27	25.60	2.30
8	17.59	0.13	15.59	0.15	37.31	0.24	16.40	1.10
14	20.50	1.20	16.11	0.17	42.30	1.70	49.00	5.20
16	19.86	0.26	16.03	0.15	39.13	0.36	19.60	1.10
21	19.26	0.27	15.98	0.18	41.16	0.50	21.10	3.40
22	17.60	0.11	15.77	0.08	37.31	0.22	62.50	5.90
23	18.17	0.15	15.83	0.10	37.72	0.26	27.22	0.86
24	17.77	0.11	15.72	0.08	37.83	0.13	36.70	3.40
28	18.74	0.28	15.77	0.08	39.67	0.43	56.40	5.50
29	20.17	0.12	16.05	0.10	41.63	0.20	34.40	2.20
33	18.44	0.26	15.93	0.16	38.05	0.40	21.80	4.40
39	19.06	0.48	15.50	0.42	39.80	0.65	3.57	0.18
43	16.81	0.11	15.72	0.10	36.53	0.19	24.20	1.90
46	18.68	0.18	15.76	0.11	38.90	0.28	20.60	2.60
148974—lithic sandstone (Curran Member, Ullawarra Formation)								
1	16.12	0.15	15.69	0.14	36.78	0.30	22.80	4.80
2	14.09	0.05	14.90	0.06	33.89	0.14	40.30	3.30
3	13.97	0.05	14.81	0.06	33.71	0.10	39.70	1.40
4	14.95	0.04	15.17	0.04	33.81	0.06	62.10	3.40
5	14.05	0.05	14.85	0.05	33.74	0.09	46.18	0.51
7	13.92	0.06	14.82	0.05	33.60	0.11	67.30	2.10
8	13.97	0.06	14.83	0.06	33.67	0.13	48.05	0.49
11	15.86	0.07	15.31	0.06	35.74	0.17	84.40	8.50
12	14.08	0.05	14.85	0.05	33.75	0.12	63.00	2.00
13	14.59	0.09	15.05	0.07	34.25	0.18	47.00	5.80
14	14.00	0.08	14.86	0.06	33.75	0.16	43.52	0.80
15	13.97	0.08	14.83	0.07	33.71	0.15	47.67	0.79
18	15.08	0.06	15.22	0.06	34.21	0.14	43.60	4.00
19	13.79	0.09	14.73	0.06	33.20	0.10	21.36	0.30
20	15.47	0.06	15.24	0.06	35.29	0.12	52.80	2.90
21	14.27	0.08	15.00	0.07	34.10	0.15	35.60	3.10
23	15.83	0.09	15.26	0.07	35.62	0.15	26.21	0.28
24	15.08	0.14	15.30	0.14	34.97	0.24	13.16	0.75
25	14.12	0.09	15.02	0.11	34.02	0.20	26.00	1.50
27	14.16	0.09	14.94	0.09	33.98	0.21	51.00	3.10
28	15.74	0.09	15.38	0.09	35.32	0.20	71.00	3.80
29	14.05	0.09	14.88	0.10	33.86	0.19	56.60	1.60
30	15.06	0.10	15.21	0.10	34.48	0.19	38.00	3.30
31	14.21	0.07	14.92	0.06	34.01	0.13	40.60	2.20
32	14.95	0.13	15.25	0.12	33.56	0.25	28.60	2.20
33	14.88	0.13	15.14	0.12	33.33	0.24	38.90	2.00
34	14.29	0.08	14.97	0.07	33.75	0.17	54.10	1.90
35	14.68	0.10	15.16	0.10	34.12	0.24	74.30	8.30
36	14.00	0.13	14.79	0.10	33.68	0.21	41.60	1.60
37	14.13	0.10	14.95	0.10	34.08	0.22	45.40	6.40
38	14.31	0.08	14.96	0.07	34.11	0.17	44.10	4.50
39	14.37	0.07	14.99	0.06	34.16	0.15	40.60	1.20
40	15.73	0.12	15.33	0.12	35.92	0.27	116.40	5.70
41	14.40	0.07	15.02	0.11	33.71	0.19	23.20	1.00
43	14.54	0.09	15.03	0.09	34.47	0.17	34.70	1.10
44	14.14	0.09	14.95	0.08	33.93	0.18	40.00	1.60
45	14.08	0.06	14.83	0.08	33.85	0.19	36.40	2.70
46	14.18	0.10	14.86	0.12	33.90	0.23	34.66	0.97
49	16.55	0.15	15.41	0.11	36.86	0.48	72.60	3.70
1820—1775 Ma Moorarie Supersuite magmatic rocks								
159996—biotite monzogranite								
1	16.33	0.15	15.47	0.13	36.00	0.28	28.20	1.70
2	16.27	0.13	15.22	0.14	36.02	0.27	29.00	1.20
3	16.65	0.14	15.51	0.10	36.05	0.25	23.80	1.60
5	16.06	0.11	15.43	0.11	35.94	0.22	50.10	2.70
6	16.76	0.15	15.49	0.15	35.88	0.20	16.01	0.46
7	16.29	0.14	15.37	0.11	36.04	0.22	15.40	0.76
8	16.22	0.12	15.41	0.10	35.99	0.20	26.00	2.00
9	16.13	0.10	15.50	0.14	36.12	0.26	20.70	1.80
11	16.85	0.15	15.83	0.14	36.67	0.24	16.90	2.10
14	16.49	0.18	15.56	0.14	36.39	0.24	15.42	0.91
18	16.67	0.10	15.65	0.15	36.59	0.20	12.20	1.00
20	16.23	0.08	15.53	0.11	36.15	0.20	26.10	1.90
23	16.56	0.16	15.57	0.15	36.47	0.24	12.65	0.97
24	16.90	0.13	15.61	0.15	36.48	0.29	14.10	1.20
25	16.27	0.10	15.48	0.10	35.95	0.18	42.70	1.50

Table 1 (*continued*)

Sample	$^{206}Pb/^{204}Pb$	$\pm2\sigma$	$^{207}Pb/^{204}Pb$	$\pm2\sigma$	$^{208}Pb/^{204}Pb$	$\pm2\sigma$	Pb (ppm)	$\pm2\sigma$
27	16.74	0.16	15.62	0.12	36.23	0.29	20.70	2.50
28	16.74	0.11	15.54	0.11	36.14	0.21	30.60	1.30
30	16.75	0.10	15.47	0.10	36.37	0.18	14.10	0.32
31	16.22	0.09	15.51	0.10	36.24	0.19	32.00	1.10
32	16.36	0.13	15.57	0.12	36.38	0.28	22.30	2.30
33	16.29	0.11	15.49	0.08	36.09	0.15	26.75	0.87
35	16.22	0.12	15.51	0.14	36.31	0.22	12.67	0.69
36	16.28	0.16	15.45	0.11	36.20	0.30	18.20	1.50
37	16.23	0.12	15.50	0.11	36.06	0.21	22.60	0.88
39	16.34	0.12	15.49	0.13	36.07	0.23	15.94	0.90
40	16.74	0.15	15.57	0.14	36.06	0.24	15.81	0.27
43	16.77	0.12	15.53	0.11	36.19	0.29	17.60	1.50
44	16.60	0.10	15.52	0.11	35.98	0.22	24.15	0.88
46	17.32	0.14	15.78	0.10	36.97	0.21	17.00	0.55
47	16.63	0.14	15.64	0.15	36.22	0.28	17.02	0.95
48	16.62	0.15	15.58	0.15	36.18	0.33	19.90	1.30
50	17.11	0.13	15.60	0.10	36.03	0.21	28.80	1.30
178024—biotite granodiorite								
2	17.08	0.37	15.90	0.38	35.48	0.58	3.79	0.27
3	17.86	0.26	15.93	0.25	37.28	0.40	6.78	0.23
4	18.37	0.22	15.93	0.13	39.08	0.32	11.26	0.25
6	17.50	0.25	15.58	0.18	36.89	0.45	7.41	0.49
7	16.86	0.17	15.46	0.11	36.33	0.26	8.29	0.36
8	17.43	0.21	15.91	0.19	36.82	0.30	7.87	0.28
9	17.55	0.46	16.05	0.34	37.51	0.71	3.62	0.36
11	17.22	0.18	15.54	0.15	36.61	0.32	11.12	0.30
12	17.31	0.29	15.74	0.27	37.58	0.36	5.27	0.58
13	19.82	0.20	16.10	0.13	37.36	0.19	12.80	1.20
15	17.95	0.34	15.80	0.23	36.76	0.38	7.96	0.92
169088—foliated biotite monzogranite								
1	16.53	0.08	15.48	0.07	35.97	0.19	120.00	6.10
2	16.60	0.10	15.51	0.10	36.00	0.21	110.70	5.10
3	16.35	0.09	15.50	0.09	35.97	0.20	109.70	7.60
4	16.22	0.07	15.45	0.06	35.71	0.12	112.60	9.70
5	16.44	0.05	15.53	0.05	35.97	0.12	119.00	12.00
6	17.13	0.08	15.61	0.07	36.32	0.17	86.30	2.00
9	17.42	0.11	15.74	0.10	36.39	0.21	55.10	3.30
11	17.14	0.09	15.63	0.08	36.26	0.20	56.40	1.60
12	16.35	0.09	15.61	0.09	36.12	0.17	84.00	10.00
13	16.41	0.09	15.55	0.09	36.10	0.19	90.00	13.00
14	17.44	0.07	15.80	0.09	36.49	0.18	46.30	4.60
15	17.15	0.07	15.67	0.07	36.47	0.15	59.80	3.80
16	17.10	0.08	15.62	0.07	36.32	0.17	54.80	2.40
17	17.54	0.12	15.90	0.12	36.77	0.22	16.60	1.10
21	16.81	0.07	15.56	0.06	36.36	0.11	98.30	1.30
23	16.76	0.17	15.72	0.14	36.24	0.27	15.99	0.42
25	16.96	0.05	15.54	0.04	36.15	0.09	66.40	1.30
28	17.68	0.08	15.75	0.07	36.57	0.16	22.20	1.70
29	17.14	0.09	15.65	0.09	36.37	0.22	89.00	3.10
30	17.17	0.08	15.59	0.07	36.22	0.14	77.90	4.70
31	16.69	0.06	15.52	0.06	36.26	0.13	110.60	4.70
32	17.05	0.06	15.55	0.07	36.18	0.14	73.16	0.96
33	16.81	0.08	15.61	0.06	36.36	0.14	103.90	5.90
34	16.92	0.09	15.60	0.09	36.37	0.20	96.50	9.30
35	16.31	0.11	15.51	0.08	35.99	0.19	24.50	3.00
36	16.57	0.09	15.46	0.08	36.18	0.18	128.40	2.40
38	16.16	0.04	15.39	0.04	35.65	0.09	92.80	4.00
39	16.15	0.09	15.44	0.08	35.74	0.18	106.00	6.60
42	16.98	0.06	15.60	0.05	36.24	0.12	104.60	5.30
43	17.25	0.09	15.64	0.07	36.20	0.16	67.60	1.70
44	17.40	0.10	15.69	0.09	36.30	0.20	63.30	4.00
45	16.64	0.11	15.63	0.09	36.43	0.22	124.10	9.20
46	16.20	0.06	15.52	0.06	35.83	0.13	116.00	15.00
47	16.03	0.06	15.47	0.06	35.60	0.14	96.00	12.00
48	16.56	0.09	15.51	0.07	36.21	0.16	73.90	4.70
49	16.75	0.06	15.49	0.06	36.12	0.14	79.70	1.20
50	16.68	0.04	15.49	0.03	36.11	0.09	127.30	5.30
1680—1620 Ma Durlacher Supersuite magmatic rocks								
178029—biotite monzogranite								
3	17.75	0.61	15.45	0.34	38.55	0.84	3.72	0.54
4	16.19	0.08	15.48	0.07	36.21	0.14	55.90	3.40
7	18.23	0.41	15.94	0.38	38.64	0.73	6.63	0.68
8	17.71	0.11	15.75	0.09	38.02	0.17	24.90	2.20
10	16.79	0.24	15.73	0.20	36.84	0.38	11.60	1.10
11	18.40	0.64	15.71	0.51	39.03	0.86	3.80	1.40

Table 1 (*continued*)

Sample	$^{206}Pb/^{204}Pb$	$\pm2\sigma$	$^{207}Pb/^{204}Pb$	$\pm2\sigma$	$^{208}Pb/^{204}Pb$	$\pm2\sigma$	Pb (ppm)	$\pm2\sigma$
13	19.42	0.67	15.88	0.09	37.91	0.17	37.40	1.70
14	17.71	0.15	15.64	0.14	37.81	0.30	45.80	3.30
Southern Pilbara granitic rocks								
195891−leucocratic monzogranite (ca. 2900 Ma)								
1	13.29	0.09	14.52	0.08	33.14	0.14	20.60	1.20
2	13.36	0.13	14.62	0.09	33.35	0.18	19.38	0.90
3	13.71	0.08	14.84	0.08	33.69	0.21	15.60	1.00
4	13.99	0.11	14.86	0.10	33.73	0.15	10.75	0.27
5	15.09	0.20	15.63	0.17	35.02	0.29	6.54	0.65
6	13.01	0.06	14.38	0.05	32.90	0.12	24.89	0.54
7	14.50	0.15	15.19	0.13	34.39	0.22	10.68	0.58
8	13.87	0.11	14.71	0.13	33.47	0.16	11.98	0.22
10	15.72	0.19	15.59	0.10	35.34	0.33	11.67	0.79
11	16.82	0.60	16.74	0.56	37.21	0.77	2.51	0.19
12	13.38	0.08	14.66	0.11	33.38	0.17	21.60	1.40
13	14.69	0.13	15.15	0.10	34.45	0.25	13.40	1.20
15	14.71	0.14	15.22	0.14	34.23	0.20	9.38	0.41
16	15.05	0.10	15.33	0.10	34.59	0.18	13.36	0.81
17	13.91	0.08	14.77	0.08	33.54	0.11	18.52	0.34
18	13.58	0.11	14.65	0.09	33.27	0.19	10.72	0.44
19	13.68	0.10	14.73	0.09	33.57	0.12	19.18	0.47
20	14.71	0.12	15.20	0.14	34.33	0.19	11.40	0.65
21	14.88	0.15	15.15	0.10	34.59	0.24	10.46	0.87
22	14.62	0.15	15.17	0.10	34.23	0.21	11.93	0.51
23	14.02	0.12	14.90	0.11	33.78	0.17	11.17	0.51
195898−leucocratic monzogranite (ca. 2900 Ma)								
1	19.92	0.11	17.02	0.08	36.35	0.17	40.40	5.80
2	17.94	0.10	16.23	0.09	35.51	0.18	45.90	4.90
3	17.88	0.10	16.21	0.09	35.74	0.19	32.40	3.80
4	18.69	0.11	16.61	0.10	36.30	0.19	25.20	2.20
5	24.20	0.97	17.40	0.15	39.95	0.61	22.40	1.70
6	22.08	0.44	16.99	0.14	40.46	0.55	42.70	3.60
7	21.72	0.66	16.93	0.12	39.79	0.78	37.60	4.00
8	21.21	0.43	16.85	0.17	39.33	0.62	14.30	1.40
9	20.21	0.09	16.97	0.09	37.06	0.17	32.50	2.50
10	18.73	0.15	16.44	0.10	36.59	0.24	59.20	3.40
11	17.48	0.10	16.05	0.09	35.52	0.20	50.60	5.90
12	17.78	0.10	16.18	0.09	35.45	0.16	34.70	3.30
13	18.41	0.13	16.33	0.10	36.05	0.25	27.50	2.30
14	17.95	0.09	16.18	0.10	35.54	0.17	24.40	1.40
15	17.85	0.11	16.09	0.10	35.41	0.18	25.50	1.70
16	18.09	0.14	16.27	0.10	35.80	0.17	19.40	1.10
17	20.29	0.18	16.64	0.09	36.91	0.23	43.50	5.50
18	18.96	0.10	16.49	0.08	36.02	0.16	37.60	4.20
19	18.63	0.08	16.37	0.07	35.73	0.13	34.10	1.70
20	18.74	0.09	16.44	0.08	35.87	0.17	36.90	1.50
21	18.23	0.09	16.27	0.06	35.82	0.15	28.60	2.40
22	20.97	0.12	17.14	0.10	37.97	0.20	28.10	3.70
23	20.42	0.30	17.07	0.11	37.29	0.17	24.60	2.00
24	17.61	0.09	16.16	0.09	35.55	0.20	23.30	1.60
25	18.12	0.16	16.43	0.12	35.51	0.24	16.30	1.10
26	18.43	0.12	16.30	0.06	36.05	0.18	32.00	1.60
27	18.16	0.09	16.29	0.09	35.84	0.16	31.40	1.50
28	18.02	0.08	16.24	0.07	35.67	0.16	38.70	2.80
29	18.21	0.12	16.26	0.10	35.77	0.19	27.90	2.20
195899−biotite monzogranite (ca. 3200 Ma)								
1	14.04	0.10	14.84	0.08	34.51	0.21	22.10	2.20
2	13.77	0.06	14.78	0.07	33.97	0.15	38.40	2.80
3	13.85	0.06	14.76	0.07	33.93	0.17	40.00	3.30
4	14.26	0.11	14.98	0.11	34.74	0.24	14.70	2.30
5	14.42	0.08	14.85	0.06	35.29	0.15	33.80	3.40
6	14.59	0.10	14.96	0.08	35.38	0.21	17.40	1.40
7	13.75	0.07	14.78	0.07	34.11	0.17	29.80	3.80
8	13.74	0.05	14.70	0.05	34.00	0.12	38.50	2.30
9	13.66	0.10	14.63	0.09	33.98	0.20	32.30	2.10
10	13.68	0.08	14.69	0.09	34.07	0.19	33.70	1.10
11	13.82	0.09	14.67	0.11	33.91	0.22	46.10	1.60
12	13.80	0.07	14.70	0.07	34.10	0.14	40.20	2.00
13	13.87	0.07	14.74	0.07	34.27	0.17	41.70	1.00
14	13.79	0.08	14.66	0.07	34.20	0.17	31.10	2.40
15	15.34	0.09	15.15	0.06	36.47	0.19	43.10	1.20
19	14.39	0.06	14.90	0.06	34.94	0.12	29.50	2.10
20	15.16	0.22	15.09	0.09	36.03	0.37	34.10	5.90
21	13.97	0.06	14.77	0.07	34.11	0.14	39.70	2.90
22	14.10	0.09	14.74	0.09	34.26	0.19	21.50	2.40
23	14.21	0.06	14.86	0.07	34.34	0.15	28.72	0.91
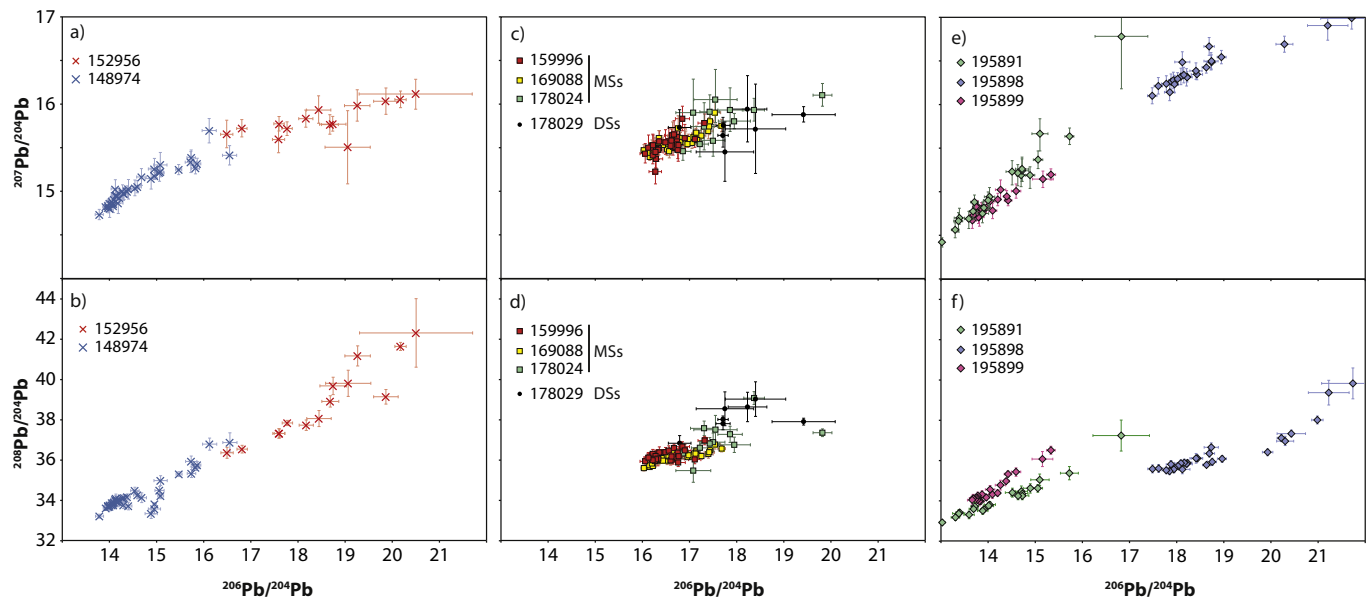
Figure 3. (a, b) Pb isotope composition of detrital K-feldspar from sedimentary rocks of the Edmund Group. (c, d) Pb isotope composition of magmatic K-feldspar from felsic magmatic rocks of the 1820–1775 Ma Moorarie Supersuite (MMs) and 1680–1620 Ma Durlacher Supersuite (DSs) of the Gascoyne Province. (e, f) Pb isotope composition of magmatic K-feldspar from felsic magmatic rocks along southern margin of the Pilbara. Uncertainties are at the 2σ level. Data are provided in Table 1.

significantly more radiogenic compositions between 4.2 and −7.2 (Fig. 4b; Cutten et al., 2016).

TIMA classification of the light fraction indicates that the sample is dominated by quartz with minor orthoclase, magnesiogedrite, albite, muscovite and ferrosaponite. Orthoclase has a median grain size of 51 μm, although many grains are much smaller, and most orthoclase grains are homogeneous. A total of 39 analyses were conducted on 39 orthoclase grains. $^{206}Pb/^{204}Pb$ ratios range from 13.8 to 16.6 with a median of 14.3. $^{207}Pb/^{204}Pb$ ratios range from 14.7 to 15.7 with a median of 15.0. $^{208}Pb/^{204}Pb$ ratios range from 33.2 to 36.9 with a median of 34.0 (Fig. 3).

4.2. Magmatic K-feldspar from the Gascoyne Province

Detrital zircon in the analysed sandstone samples 152956 and 148974, as well as siliciclastic rocks throughout the Edmund Group, are dominated by grains with U–Pb dates and Hf isotope compositions consistent with their derivation from the 1820–1775 Ma Moorarie Supersuite, and to a lesser degree, the 1680–1620 Ma Durlacher Supersuite (Fig. 4a and b). In order to test this hypothesis, magmatic K-feldspar from four typical, unaltered granitic samples (three from the Moorarie Supersuite and one from the Durlacher Supersuite) from across the Province were analysed (Fig. 1).

4.2.1. 1820–1775 Ma Moorarie Supersuite
4.2.1.1. 159996 − biotite monzogranite. This sample is a fine- to medium-grained, equigranular biotite monzogranite that locally contains sparse, 1–5 cm diameter tourmaline orbicules. Subhedral microcline phenocrysts <3 mm in length comprise approximately 1% of the rock and are set within an hypidiomorphic to anhedral groundmass of quartz (25%–30%), anhedral K-feldspar (40%), and plagioclase (10%) with minor mineral phases including biotite (5%–7%) and trace amounts of apatite, opaque minerals and titanite. U–Pb geochronology of zircon from this sample indicates a crystallization age of 1796 ± 6 Ma (Nelson, 2000), but also reveals inherited zircons with a range of Archean to Proterozoic dates and a dominant component at 2290 ± 11 Ma (Nelson, 2000). The zircon grains have a range of $\varepsilon_{Hf}(i)$ compositions between −2.0 and −6.9,

with the dominant inherited component at ca. 2290 Ma having $\varepsilon_{Hf}(i)$ compositions between −0.2 and −6.4 (Johnson et al., 2017).

TIMA classification of the light fraction indicates that the sample is dominated by quartz, orthoclase, anorthite, albite and muscovite. Orthoclase has a median grain size of 66 μm and is generally homogeneous, with the development of muscovite inclusions typically restricted to the grain margins. Twins of anorthite and patchy domains of albite are only rarely developed. A total of 32 analyses were conducted on 32 orthoclase grains. $^{206}Pb/^{204}Pb$ ratios range from 16.5 to 20.5 with a median of 18.6. $^{207}Pb/^{204}Pb$ ratios range from 15.2 to 15.8 with a median of 15.5. $^{208}Pb/^{204}Pb$ ratios range from 35.9 to 37.0 with a median of 36.2 (Fig. 3; Table 1).

4.2.1.2. 178024 − biotite granodiorite. This sample is a medium- to coarse-grained, massive granodiorite containing plagioclase (45%), quartz (30%–35%), microcline (15%), and biotite (7%–8%), with trace amounts of titanite, opaque oxide, apatite, epidote, rutile, and zircon. Plagioclase and biotite are predominantly euhedral, and are encased in an anhedral, equigranular, interlocking matrix of quartz and K-feldspar. U–Pb geochronology of zircon from this sample indicates a crystallization age of 1783 ± 5 Ma (Nelson, 2005a), and no inherited zircons were identified. Magmatic grains have a range of $\varepsilon_{Hf}(i)$ compositions between 4.4 and −5.2 (Johnson et al., 2017).

TIMA classification of the light fraction indicates that the sample is dominated by albite, anorthite, muscovite, quartz, plagioclase, clay, biotite, with only relatively minor amounts of orthoclase. Orthoclase has a median grain size of 85 μm and is generally homogeneous, although in some grains, patchy domains of albite are developed. A total of 11 analyses were conducted on 11 orthoclase grains. $^{206}Pb/^{204}Pb$ ratios range from 16.9 to 19.8 with a median of 17.5. $^{207}Pb/^{204}Pb$ ratios range from 15.5 to 16.1 with a median of 15.9. $^{208}Pb/^{204}Pb$ ratios range from 35.5 to 39.1 with a median of 36.9 (Fig. 3; Table 1).

4.2.1.3. 169088 − foliated biotite monzogranite. This sample is a fine-grained, weakly foliated monzogranite containing quartz (50%–55%), partly altered plagioclase (35%–40%), biotite (7%–8%), orthoclase (2%–3%), epidote (1%), and muscovite (1%), with trace

amounts of opaque oxide, zircon, and possible monazite. Most of the plagioclase is less than 2 mm in size, and along with locally weakly aligned biotite flakes, is enclosed in an anhedral matrix of quartz and orthoclase. U—Pb geochronology of zircon from this sample indicates a crystallization age of 1806 ± 7 Ma (Nelson, 2004). Only two inherited zircons were identified with ages of ca. 2237 Ma and 2622 Ma. The magmatic grains have a range of $\varepsilon_{Hf}(i)$ compositions between −0.1 and −6.4 (Johnson et al., 2017). The Archean inherited zircon yielded a $\varepsilon_{Hf}(i)$ composition of 0.2 (Johnson et al., 2017).

TIMA classification of the light fraction indicates that the sample is dominated by quartz, albite, anorthite, muscovite and biotite. Orthoclase comprises about 2.5% of the sample and has a median grain size of 82 μm. Orthoclase grains are predominantly homogeneous with very rare inclusions of quartz. Albite is occasionally developed in orthoclase and where present, is relatively large and at the margins of the grains. A total of 38 analyses were conducted on 38 orthoclase grains. $^{206}Pb/^{204}Pb$ ratios range from 16.9 to 19.8 with a median of 17.5. $^{207}Pb/^{204}Pb$ ratios range from 15.4 to 16.0 with a median of 15.6. $^{208}Pb/^{204}Pb$ ratios range from 35.6 to 37.2 with a median of 36.2 (Fig. 3; Table 1).

4.2.2. 1680—1620 Durlacher Supersuite
4.2.2.1. 178029 — biotite monzogranite.
This sample is a medium- to coarse-grained, porphyritic biotite monzogranite that contains abundant, equant, rounded to oval K-feldspar phenocrysts up to 3 cm in diameter. These phenocrysts are set within a medium-grained, equigranular matrix of mainly anhedral plagioclase (45%), quartz (25%), K-feldspar (25%), biotite (2%–3%), and muscovite (2%–3%), with trace amounts of fluorite, carbonate, sericite, apatite, opaque oxide, chlorite, and zircon. The K-feldspar is microcline and contains plagioclase in two forms: rounded primary inclusions from 0.2 to 1 mm in length, and as exsolution lamellae. U—Pb geochronology of zircon from this sample indicates a crystallization age of 1675 ± 11 Ma (Nelson, 2005b). Only a single inherited zircon was identified, with an age of ca. 1753 Ma. The magmatic grains have a range of $\varepsilon_{Hf}(i)$ compositions between 0.4 and −9.8 (Johnson et al., 2017), and the single inherited zircon yielded a $\varepsilon_{Hf}(i)$ composition of −1.9 (Johnson et al., 2017).

TIMA classification of the light fraction indicates that the sample is dominated by albite, quartz, orthoclase, muscovite and biotite. Orthoclase has a median grain size of 83 μm, and has albite lenses developed across the grains. A total of 8 analyses were conducted on 8 orthoclase grains. $^{206}Pb/^{204}Pb$ ratios range from 16.2 to 19.4 with a median of 17.7. $^{207}Pb/^{204}Pb$ ratios range from 15.5 to 15.9 with a median of 15.7. $^{208}Pb/^{204}Pb$ ratios range from 35.5 to 39.1 with a median of 36.9 (Fig. 3; Table 1).

4.3. Magmatic K-feldspar from the northern Capricorn Orogen

4.3.1. 195891 — leucocratic monzogranite
This sample is a medium-grained, equigranular leucocratic monzogranite containing quartz (30%), plagioclase (30%), K-feldspar (20%) and sericite (10%) with accessory clots and aggregates of iron-titanium oxides, ferruginous clinozoisite, epidote, saussurite, chlorite and biotite. Quartz and K-feldspar are generally anhedral, whereas most plagioclase is tabular showing albite twinning. Preliminary U—Pb geochronology of zircon from this sample indicates a crystallization age of 2897 ± 5 Ma. Only a single inherited zircon was identified, with an age of ca. 3168 Ma.

K-feldspar is up to 500 μm and typically do not contain any sodic intergrowths. A total of 21 analyses were made on 21 K-feldspar grains. $^{206}Pb/^{204}Pb$ ratios range from 13.0 to 16.8 with a median of 14.3. $^{207}Pb/^{204}Pb$ ratios range from 14.4 to 16.7 with a median of 15.0. $^{208}Pb/^{204}Pb$ ratios range from 32.9 to 37.2 with a median of 34.1 (Fig. 3; Table 1).

4.3.2. 195898 — leucocratic monzogranite
This sample is a medium-grained, slightly porphyritic monzogranite containing quartz (35%), K-feldspar (35%), plagioclase (25%), and biotite (5%) with accessory clots and aggregates of muscovite, iron-titanium oxides, and clinozoisite. Quartz and K-feldspar are generally anhedral and commonly the K-feldspar grains engulf zoned, clouded plagioclase crystals. Preliminary U—Pb geochronology of zircon from this sample indicates a crystallization age of 2918 ± 3 Ma. No inherited zircons were identified.

K-feldspar in this sample is typically up to 1 mm and rarely has small perthitic intergrowths which were not analysed. A total of 29 analyses were made on 29 K-feldspar grains. $^{206}Pb/^{204}Pb$ ratios range from 17.4 to 24.2 with a median of 19.1. $^{207}Pb/^{204}Pb$ ratios range from 16.1 to 17.4 with a median of 16.5. $^{208}Pb/^{204}Pb$ ratios range from 35.4 to 40.5 with a median of 36.6 (Fig. 3; Table 1).

4.3.3. 195899 — biotite monzogranite
This sample is a medium-grained, equigranular monzogranite containing plagioclase (35%), K-feldspar (30%), quartz (25%) and biotite (10%), with clots of accessory iron-titanium oxide, chlorite, and epidote. Most of the plagioclase is clouded with very fine-grained sericite, but the K-feldspar is clear and anhedral. Preliminary U—Pb geochronology of zircon from this sample indicates a crystallization age of 3239 ± 6 Ma. No inherited zircons were identified.

Feldspar grains are up to 300 μm and locally have irregular perthite intergrowths, which were avoided during analysis. A total of 20 analyses were made on 20 K-feldspar grains. $^{206}Pb/^{204}Pb$ ratios range from 13.7 to 15.3 with a median of 14.1. $^{207}Pb/^{204}Pb$ ratios range from 14.6 to 15.2 with a median of 14.8. $^{208}Pb/^{204}Pb$ ratios range from 33.9 to 36.5 with a median of 34.5 (Fig. 3; Table 1).

5. Discussion

5.1. Pb composition of the Gascoyne Province basement

Although the low U and Th contents (typically <1 ppm) in K-feldspar imply that it should record minimal radiogenic ingrowth, small variations in U or Th concentration may nonetheless result in a spread of Pb isotopic compositions along a linear array. This spread can blur distinct populations derived from different suites of magmatic rocks, decreasing the resolution of the source crustal blocks. However, in the case of the magmatic rocks from the Gascoyne Province basement, the data are relatively tightly constrained indicating little to no radiogenic ingrowth (Fig. 3).

Despite the relatively low number of magmatic samples analysed from the province, there is remarkable consistency of Pb composition within, and between, each sample (Fig. 3). The tightly constrained Pb compositions of the Moorarie Supersuite suggest that, despite the magmas complex transport and emplacement mechanisms (Johnson et al., 2017) and distance across which the samples were collected (~300 km; Fig. 1), there was either a common province-wide source of Pb to the magmatic system or all the samples have been well homogenized. With only one sample analysed from the Durlacher Supersuite, it is difficult to assess whether or not this sample is representative of the supersuite as a whole. Nonetheless, this sample was chosen because this phase is predominant throughout the northern part of the province, contains abundant K-feldspar as both phenocrysts and matrix grains, and is zircon-rich, so it would likely be strongly represented in the detritus if the province was the primary source of sediment. Since the analyses were performed on pre-existing heavy mineral separates, it was not possible to distinguish between the K-feldspar
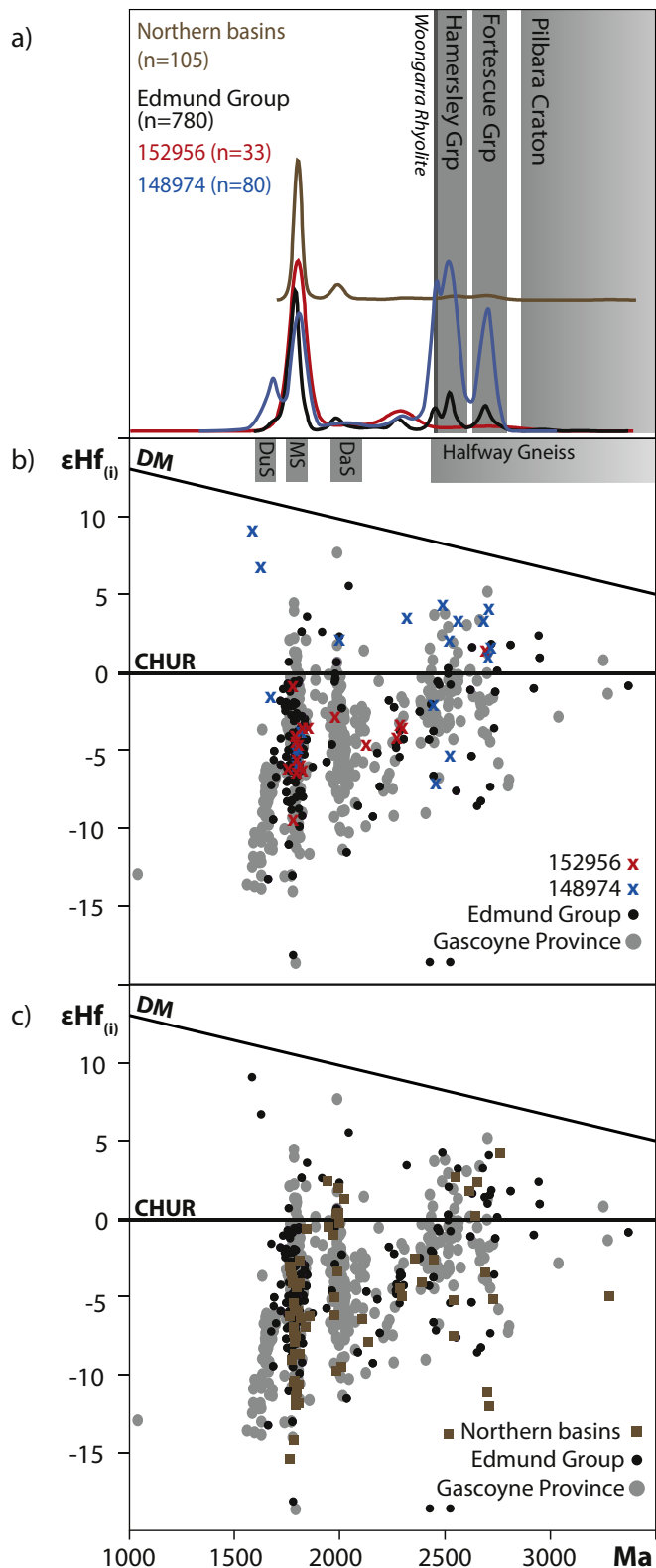
Figure 4. (a) Kernel density estimates (KDE, Vermeesch, 2012) for the age of detrital zircons from the studied samples and Edmund Group, and from older basins in the northern Capricorn Orogen including the Capricorn, Bresnahan and Mount Minnie Groups. Geochronological data are from Cutten et al. (2016). (b) $\varepsilon_{Hf}(i)$ compositions of detrital zircons from studied samples and the Edmund Group compared to magmatic zircon compositions from the underlying Gascoyne Province. (c) $\varepsilon_{Hf}(i)$ compositions of detrital zircons from the northern Capricorn Orogen basins, including the Capricorn, Bresnahan and Mount Minnie Groups, with detrital zircon data from the Edmund

phenocrysts and matrix grains, so any possible Pb composition variations between them are not known. This may account for the slightly greater variation in Pb composition, particularly in the $^{206}Pb/^{204}Pb$ ratio (Fig. 3) for this sample. Despite this, the Pb composition is still well constrained, and distinct enough from the other magmatic rocks to be recognised in any potential detrital component.

5.2. Sediment recycling the Capricorn Orogen

The presence of abundant K-feldspar in some of the Edmund Group sandstones suggests that, at least in these particular lithologies, they contain a significant component of first cycle detritus derived from igneous or metamorphic rocks. Since K-feldspar is a common rock forming mineral in many felsic plutonic rocks, which also generally contain abundant accessory zircon (as compared to, for example mafic igneous rocks), the generation of sedimentary detritus from these rocks should liberate both K-feldspar and zircon that are chemically and isotopically coupled to the host rock. The age and Hf isotopic composition of detrital zircons from the two arkosic sandstones (samples 152956 and 148974), as well as from other sedimentary rocks of the Edmund Group (Fig. 4a and b), suggest that the zircon detritus was derived predominantly from the 1820–1775 Ma Moorarie Supersuite, with minor components from the 1680–1620 Ma Durlacher Supersuite and some older rocks of the Gascoyne Province (Fig. 4b). However, the Pb isotopic compositions of the detrital K-feldspar within these sandstones do not match those from the potential granitic source rocks in the Province (Fig. 5) suggesting a more complicated source to sink pathway.

In detail, sample 152956 from the base of the Edmund Group appears to be dominated by detrital zircons from the Moorarie Supersuite with a minor older Paleoproterozoic component (Fig. 4a and b). In the $^{206}Pb/^{204}Pb$ versus $^{207}Pb/^{204}Pb$ plot (Fig. 5) there is some overlap between the composition of detrital K-feldspar grains and magmatic grains from the Moorarie Supersuite. However, in the $^{206}Pb/^{204}Pb$ versus $^{208}Pb/^{204}Pb$ graph the majority of detrital grains plot with significantly higher $^{206}Pb/^{204}Pb$ and $^{208}Pb/^{204}Pb$ ratios (Fig. 5), indicating that it is unlikely that these feldspar grains were derived from the Moorarie Supersuite. Sample 148974, from towards the top of the Edmund Group, contains a multi-modal detrital zircon age profile and Hf isotopic compositions that suggest contributions from both the Moorarie and Durlacher Supersuites, as well as older Paleoproterozoic to Archean rocks, all of which could have been sourced from within the Gascoyne Province (Fig. 4a and b). Similar to sample 152956, the Pb isotopic composition of the detrital K-feldspar grains are dissimilar to the magmatic grains, having significantly lower $^{206}Pb/^{204}Pb$, $^{207}Pb/^{204}Pb$, and $^{208}Pb/^{204}Pb$ compositions than the potential magmatic source rocks in the province (Fig. 5). These results are consistent with macroscopic paleoflow indicators such as trough cross bedding and sole marks that suggest that the majority of sediment within the group was sourced from the north and northeast or axially along the basin (Fig. 2; Martin et al., 2008), rather than from the underlying Gascoyne Province that is exposed to the south.

Potential source rocks to the north and northeast of the Edmund Group include numerous, older sedimentary basins that encompass rocks belonging to the Fortescue, Hamersley, Shingle Creek, Wyloo, Capricorn, Bresnahan and Mount Minnie Groups (Fig. 1a and b).

Group and magmatic zircon data from the Gascoyne Province. The age and Hf isotopic data are from Cutten et al. (2016). Samples 152956 (Yilgatherra Formation) and 148974 (Ullawarra Formation) are sedimentary rocks sampled from the Edmund Group.
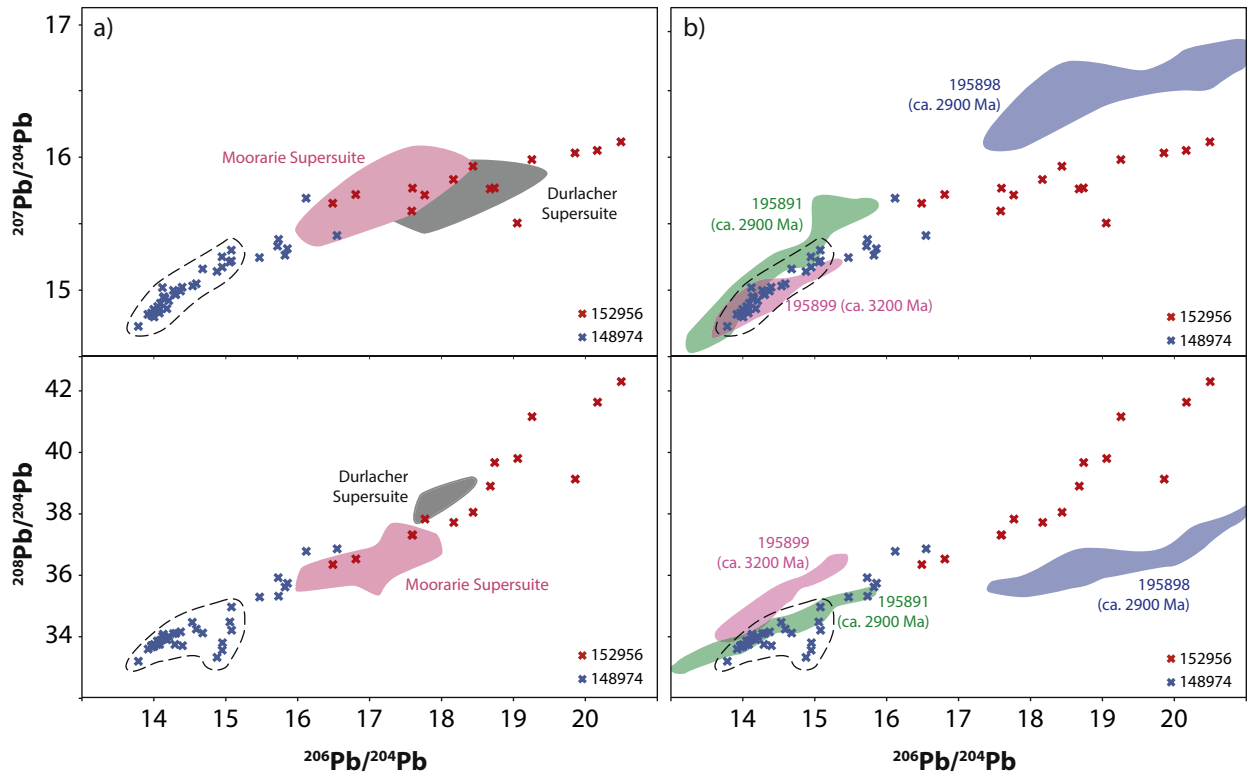
Figure 5. Summary of Pb isotope compositions of detrital K-feldspar in the studied samples versus the magmatic grains in the potential magmatic source rocks.

Although some of the basins are too old to contain detritus derived from the Gascoyne Province (particularly the Moorarie Supersuite that dominates the detritus), the Capricorn, Bresnahan and Mount Minnie Groups (Fig. 1a and b) could be potential sources as they were deposited either during, or directly after, the 1820–1770 Ma Capricorn Orogeny, but before the deposition of the 1673–1455 Ma Edmund Group (Fig. 1b; Thorne and Seymour, 1991; Hall et al., 2001). The U–Pb age and Hf isotopic composition of detrital zircon from these sedimentary rocks is remarkably similar to those in the Edmund Group and to magmatic zircon from the Gascoyne Province granitic rocks (Fig. 4a and c; Cutten et al., 2016). Therefore, it is possible that detrital zircons within these basins were derived as first cycle detritus from the Gascoyne Province during the denudation of upland regions generated during the Capricorn Orogeny. Subsequent uplift and erosion of these basins during the latter stages of the 1680–1620 Ma Mangaroon Orogeny may have recycled these zircons back toward their original source region and into the Edmund Basin.

5.3. Source of first cycle detritus into the Edmund Basin

Any primary K-feldspar liberated during the first cycle erosion of the Gascoyne Province into the northern basins (the Capricorn, Bresnahan and Mount Minnie Groups) is unlikely to have survived a second cycle of erosion, transportation and deposition, as indicated by the difference in Pb isotope compositions of the detrital and magmatic K-feldspar grains (Fig. 5). This suggests that the detrital K-feldspar present within the Edmund Group must have been generated from another primary igneous source outside the Gascoyne Province. Sources of primary igneous K-feldspar in the northern part of the Capricorn Orogen are limited as this region is dominated by sedimentary and mafic volcanic rocks (Thorne and Trendall, 2001). However, felsic plutonic, volcanic and volcaniclastic rocks are locally present. Felsic volcanic and volcaniclastic rocks, including the

2450–2445 Ma Woongarra Rhyolite (Thorne and Trendall, 2001) in the Hamersley Group, the 1804–1738 Ma Koonong Member of the Capricorn Group (Thorne and Seymour, 1991; Hall et al., 2001) and other thin, disparate felsic volcanic horizons within the Wyloo Group (Fig. 1b), are either non-K-feldspar-bearing or are generally too fine grained to yield K-feldspar crystals large enough to survive an erosion-transport-deposition cycle. However, Archean-aged, medium- to coarse-grained granitic rocks exposed in the cores of regional-scale inliers, including the Wyloo, Rocklea and Sylvania Inliers (Fig. 1a) do contain abundant, macroscopic K-feldspar, principally as a major matrix phase.

Magmatic K-feldspar from three Archean granitic rocks, one from the Wyloo Inlier and two from the Sylvania Inlier (Fig. 1a) were analysed for their Pb isotopes (Table 1). K-feldspar from all three samples show a relatively large range of Pb isotope compositions (Fig. 3e and f) that are distinct from those of magmatic K-feldspar from the Moorarie and Durlacher Supersuites but have compositions most similar to the detrital K-feldspar grains from the Edmund Group (Figs. 3 and 5). Specifically, Edmund Group sample 148974 has detrital K-feldspar grains with relatively low $^{206}Pb/^{204}Pb$, $^{207}Pb/^{204}Pb$, and $^{208}Pb/^{204}Pb$ ratios that directly overlap in composition (particularly in $^{206}Pb/^{204}Pb$ versus $^{207}Pb/^{204}Pb$ space) with magmatic K-feldspar grains from Archean samples 195891 and 195899 (Fig. 5b). Sample 152956 has detrital K-feldspar grains with relatively high $^{206}Pb/^{204}Pb$, $^{207}Pb/^{204}Pb$, and $^{208}Pb/^{204}Pb$ compositions, and although magmatic K-feldspars from Archean sample 195898 are not identical, they have a very similar range of high $^{206}Pb/^{204}Pb$ compositions (Fig. 5b). The difference in $^{207}Pb/^{204}Pb$ and $^{208}Pb/^{204}Pb$ signatures is likely due to somewhat dissimilar U and Th concentrations in the source of these feldspars. Despite these differences, as a whole the detrital K-feldspar grains in the Edmund Group best resemble Archean-aged granitic sources in the northern Capricorn Orogen.

These results suggest that any >2800 Ma-aged detrital zircons in the Edmund Group may represent a first cycle input of zircon into the Edmund Basin, particularly as zircon grains of this age are rare in the northern basins sedimentary rocks (Fig. 4a). However, out of 780 analysed zircons from the entire Edmund Group, only a very small number ($n = 30$), equating to ~4% of the total grains, yielded U—Pb dates older than ca. 2800 Ma (Martin et al., 2008; Cutten et al., 2016). Despite both samples (148974 and 152956) containing 1%—7% detrital K-feldspar grains, neither sample yielded a single detrital zircon older than ca. 2800 Ma. This suggests that not only is the zircon to K-feldspar ratio in the primary granitic source rocks very low, but that the first cycle detritus was swamped by recycled detrital zircon grains derived from the erosion of the northern basins sedimentary rocks.

5.4. Tectonic implications for the Capricorn Orogen

Newly constrained Paleo- to Mesoproterozoic source to sink relationships in the Capricorn Orogen provide robust constraints for refining the tectonic history of the region. The data indicate that during the latter stages of the extensional Mangaroon Orogeny (Sheppard et al., 2005), the northern margin of the orogen was subject to uplift and erosion. Detritus was shed toward the south into the Edmund Basin, which developed in the central part of the orogen as a continued expression of this extensional event (Cutten et al., 2016). The southern part of the orogen however, remained passive, a conclusion that could not have been made from the detrital zircon data alone. This interpretation is supported by new *in situ* U—Th—Pb phosphate dating showing that, during this event, the northern margin of the orogen was subject to repeated fault reactivation, low temperature hydrothermal fluid flow and associated gold mineralization (Fielding et al., 2017, 2018).

6. Implications for sedimentary provenance studies

We have shown that even with a comparatively limited dataset, the Pb isotope composition of detrital K-feldspar in low-grade sedimentary basins can be used in conjunction with traditional, zircon-based tools as a means to determine potential igneous source rocks. Furthermore, the Pb isotopic signature of K-feldspar may allow the first cycle component of sedimentary detritus to be more precisely identified, leading to a more complete understanding of source to sink relationships. In the case study example of the Capricorn Orogen in Western Australia, although zircon age and Hf isotopic signatures could be readily interpreted as suggesting a south to north source to sink relationship, first cycle detrital K-feldspar indicates that such interpretations are naive as sediment transport was from north to south, as illustrated by the macroscopic paleoflow indicators in the sedimentary rocks. Such dichotomy is easily reconciled by the fact that much of the detrital zircon in the basin is refractory and multicycle.

The results presented here illustrate the potential complexity in apparently simple source to sink sedimentary systems. The physical and chemical robustness of zircon, which has made it the mineral of choice for provenance studies, is also a hindrance as it may be recycled through multiple sedimentary basins (Rahl et al., 2003; Campbell et al., 2005; Dickinson et al., 2009; Dickinson and Gehrels, 2009; Hadlari et al., 2015; Anderson et al., 2016; Gagnevin et al., 2017; Lancaster et al., 2017). Without independent evidence, such as paleoflow indicators, (U—Th)/He and U—Pb 'double' dating, or detailed grain shape analyses (e.g. Markwitz and Kirkland, 2018), the erosion 'cycle' to which the detrital zircon belong may not be readily apparent and so incorrect assumptions may be made about the source to sink relationships. This has particular relevance to the provenance history of Precambrian (meta)-sedimentary basins that have been variably and multiply deformed and metamorphosed.

Appendix A. Supplementary data

Supplementary data related to this article can be found at https://doi.org/10.1016/j.gsf.2018.03.009.

References

Anderson, T., Elburg, M., Cawthorn-Blazeby, A., 2016. U—Pb and Lu—Hf zircon data in young sediments reflect sedimentary recycling in eastern South Africa. Journal of the Geological Society 173, 337—351.

Blay, O.A., Johnson, S.P., Thorne, A.M., Cutten, H.N.C., 2015. Waldburg Dolerite (P_-_wa-od). Geological Survey of Western Australia, WA. Geology Online, Explanatory Notes extract, viewed 05 December 2017. www.dmp.wa.gov.au/ens.

Campbell, I.H., Reiners, P.W., Allen, C.M., Nicolescu, S., Upadhyay, R., 2005. He—Pb double dating of detrital zircons from the Ganges and Indus Rivers: implication for quantifying sediment recycling and provenance studies. Earth and Planetary Science Letters 237, 402—432.

Cutten, H.N., Johnson, S.P., Thorne, A.M., Wingate, M.T.D., Kirkland, C.L., Belousova, E.A., Blay, O.A., Zwingmann, H., 2016. Deposition, provenance, inversion history and mineralization of the proterozoic Edmund and collier basins, Capricorn orogen. Geological Survey of Western Australia Report 127, 74.

DeWolf, P., Mezger, K., 1994. Lead isotope analyses of leached feldspars: constraints on the early crustal history of the Grenville Orogen. Geochimica et Cosmochimica Acta 58, 5537—5550.

Dickinson, W.R., Gehrels, G.E., 2009. U—Pb ages of detrital zircons in Jurassic eolian and associated sandstones of the Colorado Plateau: Evidence for transcontinental dispersal and intraregional recycling of sediment. The Geological Society of America Bulletin 121, 408—433.

Dickinson, W.R., Lawton, T.F., Gehrels, G.E., 2009. Recycling detrital zircons: a case study from the Cretaceous Bisbee Group of southern Arizona. Geology 37, 503—506.

Dixon, P.R., Lehuray, A.P., Andrye, D.M., 1990. Basement geology and tectonic evolution of Ireland as deduced from Pb isotopes. Geological Society of London 147, 121—132.

Fielding, I.O.H., Johnson, S.P., Zi, J.-W., Rasmussen, B., Muhling, J.R., Dunkley, D.J., Sheppard, S., Wingate, M.T.D., Rogers, J.R., 2017. Using in situ SHRIMP U—Pb monazite and xenotime geochronology to determine the age of orogenic gold mineralization: an example from the paulsens mine, southern Pilbara craton. Economic Geology 112, 1205—1230.

Fielding, I.O.H., Johnson, S.P., Zi, J.-W., Sheppard, S., Rasmussen, B., 2018. Neighbouring orogenic gold deposits may be the products of unrelated mineralizing events. Ore Geology Reviews 95, 593—603.

Fletcher, I.R., Farquhar, R.M., 1982. The protocontinental nature and regional variability of the Central Metasedimentary Belt of the Grenville Province: lead isotopic evidence. Canadian Journal of Earth Sciences 19, 239—253.

Flowerdew, M.J., Tyrrell, S., Riley, T.R., Whitehouse, M.J., Mulvaney, R., Leat, P.T., Marschall, H.R., 2012. Distinguishing East and West Antarctic sediment sources using the Pb isotope composition of detrital K-feldspar. Chemical Geology 292—293, 88—102.

Flowerdew, M.J., Tyrrell, S., Boger, S.D., Fitzsimons, I.C.W., Harley, S.L., Mikhalsky, E.V., Vaughan, A.P.M., 2013. Pb isotopic domains from the Indian Ocean sector of Antarctica: implications for past Antarctica-India connections. In: Harley, S.L., Fitzsimons, I.C.W., Zhao, Y. (Eds.), Antarctic Supercontinent Evolution, vol. 383, pp. 59—72.

Gagnevin, D., Tyrrell, S., Morton, A.C., Leather, J., Lee, N., Bordas-Le Floch, N., Frei, D., Lukaye, J., 2017. Sand supply to the lake Albert basin (Uganda) during the miocene-pliocene: a multiproxy provenance approach. Geochemistry, Geophysics, Geosystems 18, 2133—2148.

Hadlari, T., Swindles, G.T., Galloway, J.M., Bell, K.M., Sulphur, K.C., Heaman, L.M., Beranek, L.P., Fallas, K.M., 2015. 1.8 billion years of detrital zircon recycling calibrates a refractory part of Earth's sedimentary cycle. PLoS One 10 (12), e0144727.

Hall, C.E., Powell, C.M., Bryant, J., 2001. Basin setting and age of the late palaeoproterozoic Capricorn formation, western Australia. Australian Journal of Earth Sciences 48, 731–744.

Housh, T., Bowring, S.A., 1991. Lead isotopic heterogeneities within alkali feldspars: implications for the determination of initial lead isotopic composition. Geochimica et Cosmochimica Acta 55, 2309–2316.

Johnson, S.P., Thorne, A.M., Tyler, I.M., Korsch, R.J., Kennett, B.L.N., Cutten, H.N., Goodwin, J., Blay, O.A., Blewett, R.S., Joly, A., Dentith, M.C., Aitken, A.R.A., Holzschuh, J., Salmon, M., Reading, A., Heinson, G., Boren, G., Ross, J., Costelloe, R.D., Fomin, T., 2013. Crustal architecture of the Capricorn orogen, western Australia and associated metallogeny. Australian Journal of Earth Sciences 60, 681–705.

Johnson, S.P., Korhonen, F.J., Kirkland, C.L., Cliff, J.A., Belousova, E.A., Sheppard, S., 2017. An isotopic perspective on growth and differentiation of Proterozoic orogenic crust: from subduction magmatism to cratonization. Lithos 268–271, 76–86.

Korhonen, F.J., Johnson, S.P., Wingate, M.T.D., Kirkland, C.L., Fletcher, I.R., Dunkley, D.J., Roberts, M.P., Sheppard, S., Muhling, J.R., Rasmussen, B., 2017. Radiogenic heating and craton-margin plate stresses as drivers for intraplate orogeny. Journal of Metamorphic Geology 35, 631–661.

Lancaster, P.J., Daly, J.S., Storey, C.D., Morton, A.C., 2017. Interrogating the provenance of large river systems: multi-proxy in situ analyses in the Millstone Grit, Yorkshire. Journal of the Geological Society of London 174, 75–87.

Markwitz, V., Kirkland, C.L., 2018. Source to sink zircon grain shape: constraints on selective preservation and significance for Western Australian Proterozoic basin provenance. Geoscience Frontiers 9 (2), 415–430.

Martin, D.M., Thorne, A.M., 2004. Tectonic setting and basin evolution of the Bangemall supergroup in the northwestern Capricorn orogen. Precambrian Research 128, 385–409.

Martin, D.M., Sircombe, K.N., Thorne, A.M., Cawood, P.A., Nemchin, A.A., 2008. Provenance history of the Bangemall supergroup and implications for the mesoproterozoic paleogeography of the West Australian craton. Precambrian Research 166, 93–110.

Morris, P.A., Pirajno, F., 2005. Mesoproterozoic sill complexes in the Bangemall Supergroup, Western Australia: geology, geochemistry, and mineralization potential. Geological Survey of Western Australia Report 99, 75.

Nelson, D.R., 2000. 159996: Biotitemonzogranite, Claypan Bore; Geochronology Record 231. Geological Survey of Western Australia, p. 4.

Nelson, D.R., 2004. 169088: Foliated Biotitemonzogranite, Mundong Well; Geochronology Record 45. Geological Survey of Western Australia, p. 4.

Nelson, D.R., 2005a. 178024: Biotitegranodiorite, Minga Well; Geochronology Record 533. Geological Survey of Western Australia, p. 4.

Nelson, D.R., 2005b. 178029: Biotitemonzogranite, Coorabie Tank; Geochronology Record 538. Geological Survey of Western Australia, p. 4.

Rahl, J.M., Reiners, P.W., Campbell, I.H., Nicolescu, S., Allen, C.M., 2003. Combined single-grain (U–Th)/He and U/Pb dating of detrital zircons from the Navajo Sandstone, Utah. Geology 31, 761–764.

Reat, E.J., Johnson, C., Stearns, M., 2017. Common minerals and common Pb isotopes: uncommon applications and new method development for detrital K-feldspar provenance analysis. In: Geological Society of America Abstracts with Programs, vol. 49. https://doi.org/10.1130/abs/2017AM-297330.

Sheppard, S., Occhipinti, S.A., Nelson, D.R., 2005. Intracontinental reworking in the Capricorn orogen, western Australia: the 1680– 1620 Ma Mangaroon orogeny. Australian Journal of Earth Sciences 52, 443–460.

Sheppard, S., Rasmussen, B., Muhling, J.R., Farrell, T.R., Fletcher, I.R., 2007. Grenvillian-aged orogenesis in the palaeoproterozoic Gascoyne complex, western Australia: 1030–950 Ma reworking of the proterozoic Capricorn orogen. Journal of Metamorphic Geology 25, 477–494.

Thorne, A.M., Seymour, D.B., 1991. Geology of the Ashburton basin, western Australia. Geological Survey of Western Australia Bulletin 139, 141.

Thorne, A.M., Trendall, A.F., 2001. The geology of the Fortescue group, Pilbara craton, western Australia. Geological Survey of Western Australia Bulletin 144, 249.

Tyrrell, S., Daly, J.S., Kokfelt, T.F., Gagnevin, D., 2006. Common-Pb isotopic composition of detrital K-feldspar grains: validation as a provenance tool and its application to Upper Carboniferous paleodrainage, Northern England. Journal of Sedimentary Research 76, 324–345.

Tyrrell, S., Haughton, P.D.W., Daly, J.S., 2007. Drainage re-organization during break-up of Pangea revealed by in-situ Pb isotopic analysis of detrital K-feldspar. Geology 35, 971–974.

Tyrrell, S., Leleu, S., Souders, A.K., Haughton, P.D.W., Daly, J.S., 2009. K-feldspar sand-grain provenance in the Triassic, west of Shetland: distinguishing first-cycle and recycled sediment sources? Geological Journal 44, 692–710.

Tyrrell, S., Haughton, P.D.W., Daly, J.S., Shannon, P.M., 2012. The Pb isotopic composition of detrital K-feldspar: a tool for constraining provenance, sedimentary processes and paleodrainage. In: Sylvester, P.J. (Ed.), Quantitative Mineralogy and Microanalysis of Sediments and Sedimentary Rocks, MAC Short Course Ser, vol. 42. Mineral. Assoc., Québec, Canada, pp. 203–217.

Vermeesch, P., 2012. On the visualisation of detrital age distributions. Chemical Geology 312–313, 190–194.

Wingate, M.T.D., 2002. Age and Palaeomagnetism of Dolerite Sills of the Bangemall Supergroup on the Edmund 1:250 000 Sheet. Geological Survey of Western Australia, Western Australia, p. 48. Record 2002/4.

Woodhead, J.D., Hergt, J.M., 2001. Strontium, Neodymium and Lead isotope analyses of NIST glass certified reference materials: SRM 610, 612, 614. Geostandards and Geoanalytical Research 25, 261–266.

Zartmann, R.E., Wasserburg, G.J., 1969. The isotopic composition of lead in potassium feldspars from some 1.0-b.y. old North American igneous rocks. Geochimica et Cosmochimica Acta 33, 901–942.

Zhang, Z., Tyrrell, S., Li, C., Daly, S., Sun, X., Li, Q., 2014. Pb isotope compositions of detrital K-feldspar grains in the upper-middle Yangtze River system: implications for sediment provenance and drainage. Geochemistry, Geophysics, Geosystems 15, 2765–2779.

Zhang, Z.J., Tyrrell, S., Li, C.A., Daly, J.S., Sun, X.L., Blowick, A., Lin, X., 2016. Provenance of detrital K-feldspar in Jianghan basin sheds new light on the pliocene-pleistocene evolution of the Yangtze river. The Geological Society of America Bulletin 128, 1339–1351.

Zhang, Z., Daly, J.S., Li, C.A., Tyrrell, S., Sun, X.L., Yan, Y., 2017. Sedimentary provenance constraints on drainage evolution models for SE Tibet: evidence from detrital K-feldspar. Geophysical Research Letters 44, 4064–4073.

Zi, J.W., Rasmussen, B., Muhling, J.R., Fletcher, I.R., Thorne, A.M., Johnson, S.P., Cutten, H.N., Dunkley, D.J., Korhonen, F.J., 2015. In situ U–Pb geochronology of xenotime and monazite from the Abrapolymetallic deposit in the Capricorn Orogen, Australia: dating hydrothermal mineralization and fluid flow in a long-lived crustal structure. Precambrian Research 260, 91–112.